

# Transient discharges from marine hydrocarbon seeps: spatial and temporal variability

I. Leifer · J. R. Boles · B. P. Luyendyk · J. F. Clark

**Abstract** Marine hydrocarbon gas emissions at an intense, 20-m-deep seep in the Santa Barbara Channel, California were studied with a network of three turbine seep-tents and repeated seabed mapping. The tents observed two gas ejection events that are interpreted as due to blockage of constrictions in fractures and subsequent blow-through. Seabed mapping suggests that very large transient emission events occur, are related to tar, and are temporally and spatially variable. Transient emissions have the potential to more efficiently transport methane to the atmosphere than steady-state emissions. We present an electrical model analog of subsurface seepage useful for seepage flux interpretation. The model predicts that variations in resistance at one vent shifts some of its flux to other connected vents, and that the shift is not zero-sum, i.e., a resistance change at one vent causes a flow change for the overall fracture system.

**Keywords** Hydrocarbon migration · Marine seeps · Bubble

## Introduction

The global flux of methane to the atmosphere is of interest because it is a potent greenhouse gas, at least twenty times more effective in radiative heating than carbon dioxide. Also, its atmospheric levels have risen for the last century

(Rowland 1985). It is estimated that at present 535 Tera-grams (Tg; 1 Tg=10<sup>12</sup> g) enters the atmosphere annually of which 375 Tg are from anthropogenic and 160 Tg from natural sources (Prather and others 1995). The majority of natural methane is biogenic, whereas thermogenic or geologic methane, which is <sup>14</sup>C depleted, accounts for only ~20% of present sources (Cicerone and Oremland 1988; Quay and others 1999). The most significant natural sources today are tropical and northern high latitude wetlands, which provide ~70% of the natural budget or ~115 Tg yr<sup>-1</sup> (Prather and others 1995). Estimates by Crutzen (1995) suggest these wetland sources may be significantly larger than previous estimates. Other natural methane sources include continental and marine hydrocarbon seepage (Hovland and others 1993; Hornafius and others 1999; Milkov 2000), methane emitted from the decay of organic matter in marine sediments (Judd and Hovland 1992; Hovland and others 1993), fires, termites, lakes, and enteric fermentation in animals (Prather and others 1995).

Although the contribution to the atmosphere from geological sources is generally considered small, recent estimates suggest marine seeps contribute a conservative 20 Tg yr<sup>-1</sup> (Kvenvolden and others 2001). Marine seeps account for only part of the global geological methane emissions, estimated at 30–70 Tg yr<sup>-1</sup> (Etiope and Klusman 2002). One of the difficulties with determining the contribution of marine seeps to the atmospheric methane cycle is that the fate of gas phase (bubble) methane from seeps or methane hydrate dissociation (Kennett and others 2003) remains largely unknown. A key issue is what fraction of methane escaping at the seabed enters the atmosphere. Because the ocean is undersaturated in methane, methane dissolution occurs rapidly (Clark and others 2003). Although much of the methane emission from hydrates may dissolve in the deep ocean, evidence exists that hydrate seep bubbles from 550 m in the Gulf of Mexico reach the mixed layer (De Beukelaer and others 2003). Not only is assessment of current emissions to the atmosphere important, but predictions of future emissions due to global climate change are needed. Warmer ocean waters likely will increase hydrate dissociation, thereby releasing more methane. The Clathrate Gun Hypothesis invokes this mechanism to explain some geological evidence (Katz and others 1999; Kennett and others 2000, 2003). However, predicting the effect of hydrate dissociation on methane flux to the atmosphere depends upon many poorly

Received: 20 September 2003 / Revised: 22 June 2004  
Accepted: 20 April 2004  
Published online: 17 September 2004  
© Springer-Verlag 2004

I. Leifer (✉)  
Marine Sciences Institute, University of California,  
Santa Barbara, CA 93106, USA  
E-mail: ira.leifer@bubbleology.com

J. R. Boles · B. P. Luyendyk · J. F. Clark  
Geological Sciences, University of California,  
Santa Barbara, CA 93106, USA

quantified and poorly understood aspects of seep bubble plumes. This underscores the importance of understanding processes associated with marine seep gas bubbles. Many factors affect the fate of seep bubbles rising from a given depth and thus their methane flux to the atmosphere. The most important are bubble size and the interaction of the bubbles with the local ocean environment (Leifer and others 2000b; Clark and others 2003). As a result, transient events that temporarily increase the gas flux by orders of magnitude can significantly alter the fate of seep gases. Unfortunately, although evidence shows that transient events occur (Tryon and others 1999; MacDonald and others 2000), quantitative observations are absent, particularly with regards to magnitude, bubble size distribution, temporal and spatial frequency of events, and modification of the local oceanic environment. All these aspects must be understood to assess the contribution of transient events to global budgets. In this paper the authors present observations using two new seep measurement approaches that provide evidence of the temporal and spatial variability in marine seepage and of transient emissions in particular.

## Factors affecting the fate of marine seep gas

Marine seep bubbles contribute to methane budgets in three different regions, (1) dissolution in the deep-sea, (2) transport to the surface mixed-layer, and (3) transport to the atmosphere. For methane that has dissolved into the deep ocean, the diffusion time scale to the atmosphere is long, ~50 yr, (Rehder and others 1999) compared with microbial oxidation, <1 year, (Watanabe and others 1995; Tsunogai and others 2000; Valentine and others 2001). Thus deep-sea dissolution of seep gas does not affect atmospheric budgets, although it provides an energy source for deep-sea ecosystems, particularly chemosynthetic communities such as found at seepage sites (MacDonald and others 1989). Where bubbles survive transit to the sea surface, their remaining methane directly contributes to global atmospheric budgets. When bubbles dissolve in the mixed-layer, some fraction of the methane dissolved into the mixed-layer can transfer to the atmosphere by air-sea gas exchange. And finally, because seep bubble-plumes are associated with upward fluid motions driven by the buoyant rise of the bubbles—the upwelling flow—(McDougal 1978; Leifer and others 2000b; Leifer and MacDonald 2003), dissolved methane in the bubble plume is vertically transported (Leifer and Judd 2002). This allows some of the methane-enriched water in the plume below the mixed-layer to be transported into the mixed-layer where it can potentially escape to the atmosphere. Thus, understanding the fate of seep gas requires the understanding of bubble processes and bubble-plume processes in the ocean.

As a bubble rises, the outflow of methane (and other hydrocarbon gases, if present) is driven by the concen-

tration difference with the surrounding fluid (Leifer and Patro 2002):

$$dn/dt = k_B(r) 4 \pi r^2 (C - HP) \quad (1)$$

where  $n$  is the molar content of the bubble,  $t$  is time,  $k_B$  is the individual bubble gas transfer rate,  $r$  is the equivalent spherical bubble radius,  $C$  is aqueous concentration,  $H$  is the Henry's Law constant (Wanninkhof 1992), and  $P$  is the partial pressure for each gas. From (1) the outflow rate is dependent upon  $r$ , the concentration difference between the bubble and the surrounding water ( $C - HP$ ), and factors affecting  $k_B$ . Parameters affecting  $k_B$  include gas diffusivity, temperature, and  $r$  (Clift and others 1978; Leifer and others 2000a). Also, factors that affect the bubble's boundary layer—i.e., bubble hydrodynamics—are important including, surfactant (surface-active substance) contamination (Patro and others 2001), oil (MacDonald and others 2002), turbulence from other bubbles (Gal-Or and Waslo 1968), and hydrate skins (Rehder and others 2002). Larger bubbles with their greater volume transport more methane and a greater fraction of their initial methane to shallower depths, while smaller bubbles dissolve at deeper depths (MacDonald and others 2002). Thus, bubble size is critical to predicting the fate of the seep gas. For example, for clean—uncontaminated—methane bubbles rising from 100 m, bubbles with  $r = 1,000, 3,000, 5,000,$  and  $10,000 \mu\text{m}$  transport 0.01, 5, 30, and 70% of their methane to the atmosphere, respectively (from Leifer and Patro 2002).

In addition to the above mentioned factors, bubble plume processes affect the bubble gases' fate, by elevating  $C$  in the plume water above background (decreasing  $C - HP$ ) and by creating an upwelling flow. Since bubbles rise relative to the surrounding fluid (Woolf and Thorpe 1991), the upwelling flow decreases the time for bubbles to reach the mixed-layer or sea surface. Seep upwelling flows were observed at both 550-m deep seeps in the Gulf of Mexico (Leifer and MacDonald 2003) and at shallow seeps at 20 to 70 m deep in the Santa Barbara channel (Leifer and others 2000b; Clark and others 2003). Elevation of  $C$  in seep bubble plume water was reported in the Santa Barbara Channel (Leifer and others 2000b; Clark and others 2003). These effects result from the cumulative effect of all the bubbles in the plume; thus, they depend on the total emission flux (Leifer and others 2000b) and the bubble size distribution (Leifer and Patro 2002).

## Bubble size-distribution observations

In the following discussion we define vents as high flow and low flow based on the characteristics of the produced bubble distributions. This distinction is based on laboratory observations of bubbles produced from drawn capillary tubes in a tank. At low flow rates, the bubble size depends only on the capillary tube diameter

and is independent of the gas flow rate (Blanchard and Syzdek 1977). Thus an increase in flow increases the rate bubbles are produced, not their size. At high flow rates, bubble size increases with flow, and in the formation process bubbles spanning a wide size range are produced (Slauenwhite and Johnson 1999). In the transition regime a few smaller and larger bubbles are produced. Vents in this transition regime are classified as low flow. The limited field data agrees well with laboratory observations.

Leifer and MacDonald (2003) reported seep-bubble size-distributions from exposed hydrate in the Gulf of Mexico at 550-m depth emitted from three seep vents. Reported distributions were narrow and sharply peaked, or broad. The two narrow and sharply peaked distributions were produced by low flow vents, while the high flow vent produced a broad, shallow distribution spanning from very large bubbles ( $r > 1$  cm) to small bubbles at the minimum size resolution limit. Leifer and Judd (2002) reported a narrow peaked distribution at the sea surface in the Santa Barbara Channel. Currently, there are no other published seep-bubble size-distributions.

### Seep upwelling observations

Rising bubbles vertically accelerate the surrounding fluid, creating an upwelling flow, which decreases the bubble transit time across the water column, thereby enhancing vertical bubble-mediated methane transport (Leifer and Patro 2002). Leifer and others (2000b) reported seep upwelling velocities in the Coal Oil Point (COP) Seep Field determined by visually tracking the rise of fluorescein dye injected two meters below the sea surface. Velocities varied from  $15 \text{ cm s}^{-1}$  for a very weak seep that produced only a few tens of bubbles per second to  $\sim 1 \text{ m s}^{-1}$  for the largest seep in the field, the Seep Tent Seep ( $\sim 70$ -m depth,  $34^\circ 23.074' \text{N}$ ,  $119^\circ 53.388' \text{W}$ ). Leifer and MacDonald (2003) inferred the upwelling flow for bubble streams from exposed hydrate at 550 m in the Gulf of Mexico with measurements of the bubble vertical velocities. Upwelling velocities were  $20 \text{ cm s}^{-1}$  for the high flow vent, and  $5 \text{ cm s}^{-1}$  and  $< 2 \text{ cm s}^{-1}$  for two low flow vents, the latter of which produced very oily bubbles. Upwelling flow velocities in the water column are likely larger than near the seabed where the seawater is under acceleration. If the bubble plume survives to the sea surface, then the upwelling flow decelerates near the sea surface where it must diverge. Clark and others (2003) reported on total water column upwelling flows at a very active seepage area, Shane Seep (22-m depth,  $34^\circ 23.370' \text{N}$ ,  $119^\circ 53.428' \text{W}$ ) in the COP Seep Field. The upwelling velocity was measured by releasing fluorescein dye into the bubble stream at the seabed, and measuring the time to reach the sea surface. The maximum upwelling velocity occurs along the plume axis (McDougal 1978). Based on the initial arrival of the dye at the surface, the velocity was  $\sim 40 \text{ cm s}^{-1}$ . Clark and others (2003) proposed that seeps modify their environment thereby increasing the methane flux to shallower depths (i.e., to the mixed-layer and/or to the atmosphere).

## Transient gas emissions and seep-bubble transport to the atmosphere

Given the seep depth, emission bubble size-distribution, and ambient plume conditions such as dissolved plume gas concentrations, a numerical bubble model can predict the methane dissolution rate at different depths, or the fraction that reaches the atmosphere, enters the mixed-layer, and dissolves in the deep-sea. From this the global flux to the atmosphere could be estimated if the distribution of seepage in continental shelf waters was known. However, quantitative measurements of these parameters, even for steady-state seepage, are few to non-existent. In addition, seepage varies on time scales from decadal (Fischer and Stevenson 1973; Fischer 1978; Quigley and others 1999) to tidal (Boles and others 2001) and sub-hourly (Leifer and Boles 2004a). Seepage also varies spatially (Quigley and others 1999; Hornafius and others 1999; Washburn and others 2001; 2004). These temporal variations result from either external cyclical forcings, such as tides and swell, or other non-cyclical factors such as the interaction between gas and oil fluxes (Boles and others 2001; Leifer and others 2003; Leifer and Boles 2004b). Furthermore, indirect observations exist of “eruptive” gas emissions from marine (Tryon and others 1999; MacDonald and others 2000) and terrestrial seeps and mud volcanoes (Sokolov and others 1969). We term these emissions “transient”. Moreover, seepage associated features such as pockmarks and mud volcanoes are observed globally (Judd and others 2002) and suggest transient gas emissions occur with non-negligible frequency. The general lack of quantitative seepage values for steady state (including cyclical) seepage not to mention transient events, presents a challenge to estimating the global contributions from non-transient and transient marine seepage (e.g., Milkov and others 2003).

In this paper we present evidence that in active seepage areas in the Coal Oil Point (COP) Seep Field, transient gas emissions occur frequently. Based on observations (both published and presented below) we propose that these emissions are more likely to transport methane to the atmosphere for three reasons. For transient emissions, (1) bubbles are larger, (2) upwelling flows are produced, and (3) plume water becomes saturated. Failure to account for the transient contribution, including these effects of plume ambient condition modifications, will likely lead to underestimation of the total marine seep contribution to atmospheric methane budgets.

## Materials and methods

### Methods overview

Given the spatial and temporal variability of gas seeps, measurement approaches that provide both spatial and temporal data are needed. Methods discussed in this paper include a turbine seep-tent for measuring gas flux and

seabed mapping. These methods were tested in the COP Seep Field, located near the University of California, Santa Barbara (UCSB). The field has a wide diversity of seepage rates and thus provides an *ideal natural laboratory* for studying seep processes and developing measurement instruments and techniques.

### Turbine seep-tent flux monitor

The underlying principle of the turbine seep-tent (Fig. 1) is that rising bubbles generate an upwelling flow that can be measured by the spin rate of a turbine (Leifer and Boles 2004a). In brief, a 2-m diameter conical tent of thin polyvinylchloride (PVC) plastic collects bubbles which are funneled through a breakup grid into a chimney where the turbine is mounted. Since the upwelling flow depends in part on bubble size, the grid ensures an approximately constant bubble size, as well as preventing debris from entering and jamming the turbine. Magnets on the turbine shaft generate pulses (four per rotation) in a Hall effect sensor. A data logger (OMP-MODL, Omega Corporation, CT) recorded the number of pulses per time interval. The time interval was chosen so that several pulses were recorded per interval to maximize the time resolution (0.2 s). Temperature and pressure were recorded with a 3-s time interval by a conductivity temperature device (CTD) with internal data logging capabilities (SB-39, Seabird, FL) mounted on one tent frame.

Since the pulse series is quantized, data was 1-s (i.e., 5 intervals) running averaged and then 1-s block averaged. De-quantized series were converted to a gas flux with a function (see Fig. 2) determined from a series of calibration experiments in the 3×5×52 m wind-wave channel of the UCSB Ocean Engineering Laboratory. In these experiments, bubbles were created by connecting an air compressor to a regulator and then one of a series of rotameter flow controllers (Omega Corporation, CT). A tube then ran from the flow controllers to the wave-tank bottom where it was either connected to one of two air stones or left unconnected. Three distinct bubble size-distribution streams were produced. The flow at the turbine was corrected using Boyle's law for the hydrostatic pressure

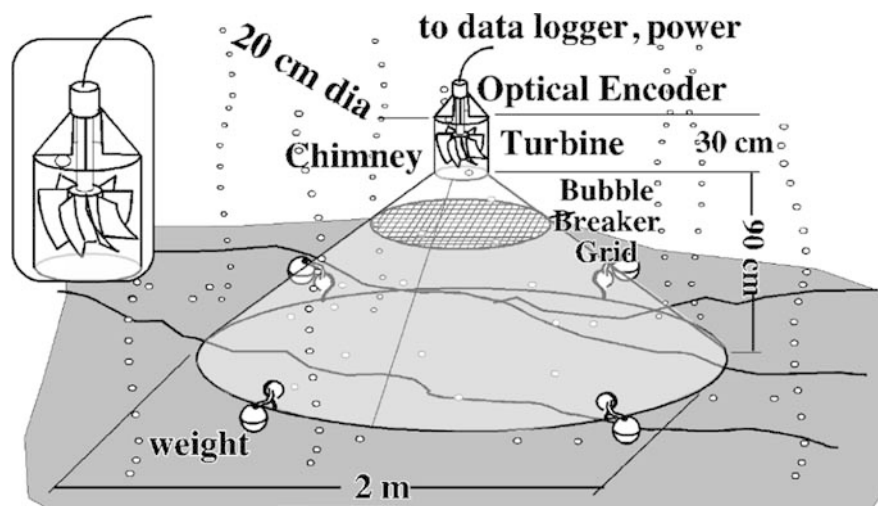


**Fig. 1**  
Turbine seep-tent schematic. *Inset* shows turbine details

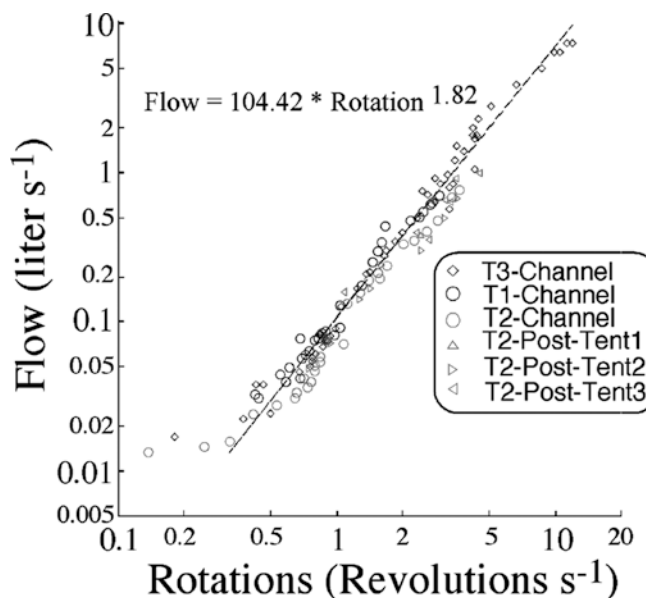


**Fig. 2**  
Flow rate as a function of rotation rate for the turbine seep-tent calibration experiments. *Line* shows the least-squares, linear-regression analysis fit to data over the range of the fit. Data key on figure. T1 – T3 are for the three aerators, “no tube”, “small bubbles,” and “large bubbles,” respectively

difference between the air stone and turbine. For all three-bubble sources there was very good correlation in gas flux ( $R^2=0.985$ ) spanning nearly four orders of magnitude. Post mission calibration (Fig. 2) agreed well with the pre-mission calibration. Calibration also showed tent tilt negligibly affected turbine efficiency flux for small ( $<10^\circ$ ) tilt angle (Leifer and Boles 2004a).

### Seabed mapping

For 3 years (2000–2003), SCUBA divers periodically visited an area of very active seepage, Shane Seep, and conducted both video and measurement surveys, documenting numerous changes in seabed morphology. Since the seabed in the area of the COP seeps is generally

featureless sand—excepting the seeps (Fischer 1978), north–south and east–west steel-link transect chains (2.5-cm links, 20-m long) were laid down late October 2001. Heavy chains allowed the transects to survive winter storms. The chains were centered on a position 3.5-m west–northwest of two prominent “hydrocarbon volcanoes”. These volcanoes are termed hydrocarbon (HC) volcanoes to denote that the volcano walls are a combination of tar and sand rather than mud (La Montagne and others 2004). HC volcanoes generally had an associated active major vent (high flow) and were marked by closed cell foam numbers. Surveys used a measuring tape to determine distances to major morphological features, wall heights, and volcano dimensions. Volcano depths were measured using a level and ruler. In the November 2003 survey, the depth at key locations was determined with a dive watch ( $\pm 15$  cm) to quantify regions of seabed uplift or depression.

### Site description

The COP Seep Field is probably the best-studied seep field in the world, and is shown in Fig. 3. Studies have quantified seep area (e.g., Allen and others 1970; Fischer and Stevenson 1973; Fischer 1978; Hornafius and others 1999) and emission fluxes using sonar techniques, ocean geochemistry, and direct gas capture at the sea surface. During the last 7 years, the UCSB seep group has mapped the seeps in the area using sonar images and quantified seepage flux from sonar and direct gas capture using a flux buoy (Washburn and others 2001; 2004). Results indicate

that  $\sim 1.5 \times 10^5 \text{ m}^3 \text{ day}^{-1}$ — $4.5 \times 10^{10} \text{ g yr}^{-1}$ —of seep gas is emitted to the atmosphere from  $\sim 3 \text{ km}^2$  of sea floor (Hornafius and others 1999) with roughly an equal amount dissolved into the coastal ocean (Clark and others 2000). The seeps also release about 80 barrels oil  $\text{day}^{-1}$  -  $5 \times 10^6 \text{ l yr}^{-1}$  (Clester and others 1996) with oil slicks a common channel feature. It has been noted that oil (Mikolaj and Ampaya 1973) and gas (Boles and others 2001) emissions vary with tides. Quigley and others (1999) noted seepage changes on decadal time scales in the field with significant decrease in seepage area between 1973 and 1995.

Seep locations are controlled by faulted anticlines (Fischer 1978) and lie along three water depth trends. The inner trend is SCUBA-diver accessible, depth  $\sim 20$  m, and includes Shane Seep and IV Super Seep. A second trend at depth  $\sim 40$  m includes the Horseshoe seeps and COP Seeps. The deepest trend (depth  $\sim 70$  m) includes La Goleta Seep and the Seep Tent Seep as well as Platform Holly. All seep names are informal.

## Observations

Shane Seep was chosen for this study for several reasons. Shane Seep has the most intense and concentrated seepage in the seep field, with the highest single point flux measurements, the third highest overall flux (Washburn and others 2004), and is diver accessible. Seabed surveys show

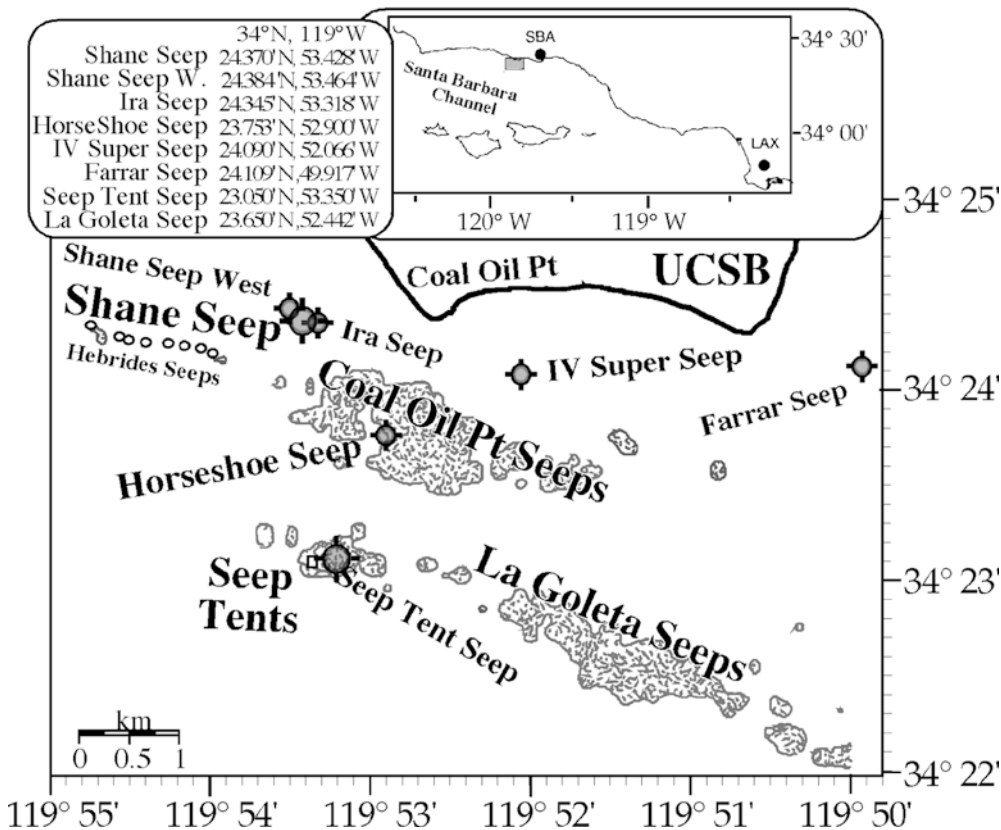


**Fig. 3**

Location of informally named seeps in the Coal Oil Point Seep Field, Santa Barbara Channel off the coast of Santa Barbara, California. *Upper right panel* shows the southwest US coast; *upper left panel* shows the Santa Barbara Channel with gray rectangle indicating the location of the study area, shown in *lower panel*. Gray areas in *lower panel* indicate regions of high bubble density from sonar returns (Hornafius and others 1999). Inshore seeps (Shane Seep, IV Super Seep, and Farrar Seep) were too shallow for the survey. SBA is Santa Barbara airport, LAX is Los Angeles airport

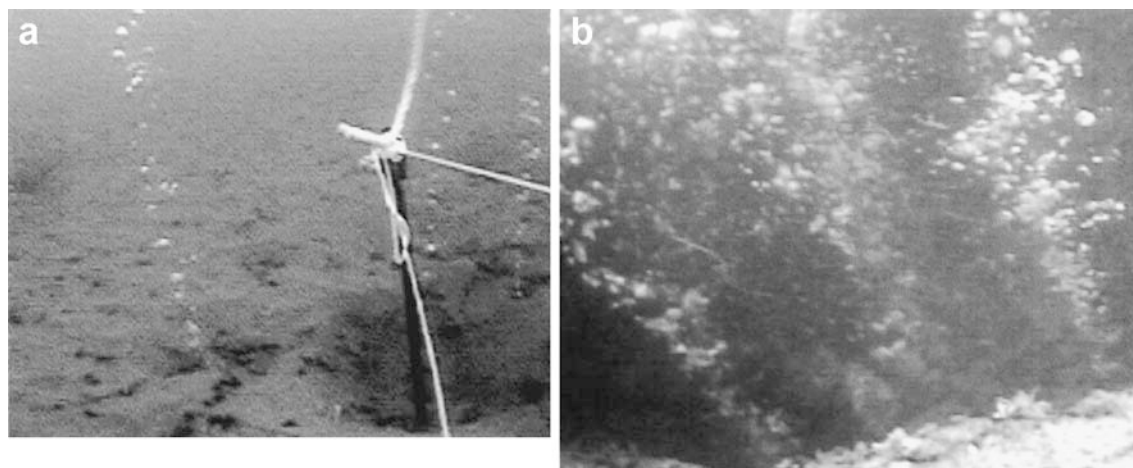


**Fig. 4**

Images from Shane Seep taken Nov. 2000. **A** shows peripheral region 10 m north of the transect line center. Sand anchor extends ~50 cm above the seabed. **B** shows main vent in HC volcano #1. HC volcano rim is visible to lower right. Width of image is approximately 1 m, the largest bubbles are 2–3 cm across

seepage spanning a wide range of fluxes and bubble stream types, from streams separated by 1–2 m in the peripheral zone that emitted bubbles in lines (See Fig. 4A), to very intense vents producing fist sized bubbles every few tenths of a second in the HC volcanoes (See Fig. 4B). Figure 5 summarizes the seabed mapping observations from November 2000 to November 2003.

#### Seabed morphology variations over time

##### Seep-scale nomenclature

As is typical for many natural systems, the COP Seep Field seepage exhibits spatial structures on diverse scales, from kilometer to centimeter. Since the processes controlling these features are different, we introduce the following nomenclature to distinguish between seepage at different scales (Leifer and Boles 2004b). The largest scale is the seep field. Seep fields are isolated from each other by large distances (large is defined as >20 times the size scale of the structure, in this case, the seep field). Within the seep field are active seep areas, which are surrounded by areas without seepage. Seep areas often are controlled by the underlying geological structures (faults, fractures, salt diapirs, caprocks, etc.) and may span several to tens (or even hundreds) of meters. A seep area may contain one or more central seep zone or zones, which are defined by distinct morphological features (mud volcanoes, mounds, brine pools, gryphons, etc.). Each central zone is generally surrounded by a peripheral seep zone, which is much less active and is absent significant features. Although a seep area can contain multiple central seep zones or none, we defined the entire peripheral area as a single zone. At the smallest scale (neglecting microseepage) is the seep vent, from which bubbles emerge at a single point. Finally, structures larger than seep vents may exist within seep zones and are termed seep domains. We define the seep domain as including vents that exhibit close intercon-

tedness. Thus flux variations at one vent strongly affect the flux at other vents in the domain. Furthermore, some vents in one seep domain may be physically located in another seep domain; it is the connectivity that is important.

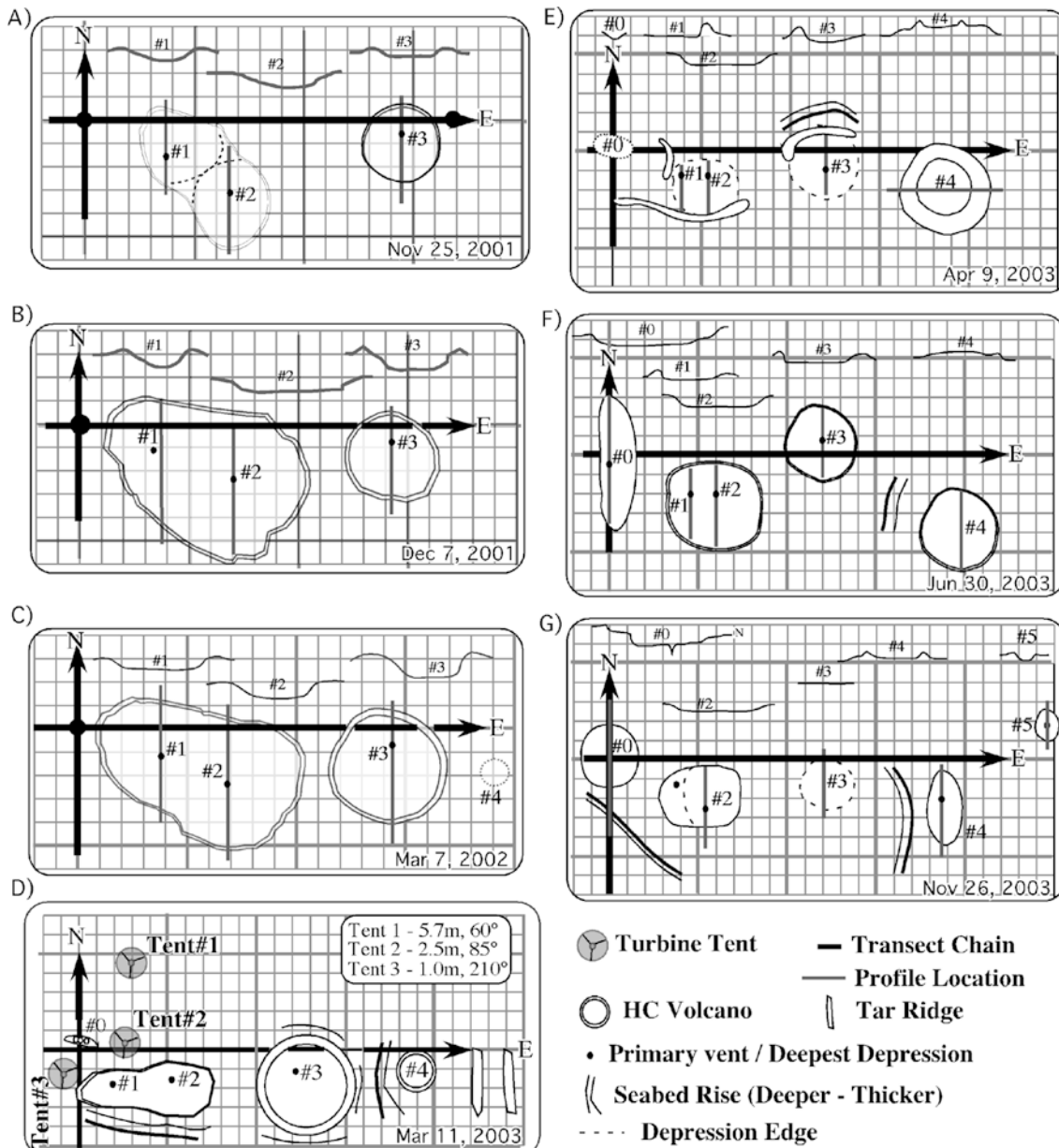
##### Seabed surveys

Video surveys from November 2000 showed just two HC volcanoes (#1 and #2) with a dividing ridge between them, (indicated by a dashed line in Fig. 5A). The volcanoes were roughly circular and ~3 m in diameter. Few changes were noted during the next year. The first survey when seabed features were measured was November 25, 2001. Over the subsequent 2 years, numerous changes occurred including: appearance of new volcanoes and other seep related features, growth of walls, destruction of walls, relocation of volcanoes, and plastic-like seabed deformations (see Table 1).

The most significant change observed was the formation of HC volcano #3. HC volcano #3 was nearly circular and appeared during a 3-week period in October 2001 after the transect chain was laid in place. During the same 3-week period, the walls of HC volcanoes #1 and #2 were partially destroyed. HC volcano #3 became the dominant seepage zone until HC volcano #0 became dominant in June 2003. Finally, by November 2003, HC volcano #3 became inactive with only trace remnant features (slight depression, dark sand coloration).

The formation of active HC volcanoes #4 and #0 both were presaged by the appearance of minor seepage related features in March 2002 and March 2003, respectively. This may have happened for HC volcano #3, but was not noted (once it was recognized that major features may be presaged by the appearance of small features, subsequent surveys were conducted more carefully). In some cases, the appearance of small intense seepage features did not presage the appearance of a HC volcano. In June 2003, a small, low-activity HC volcano ~75 cm in diameter and ~5 cm deep was first noted ~3 m west of the mooring point (but not mapped). It was not noted in a subsequent survey in November 2003.

Also observed in association with rapid growth of HC volcanoes was a change in the volcano floor from sand to exposed stones and large tar blocks. When first surveyed

**Fig. 5**

Results of Shane Seep seabed surveys 11/2000–11/2003. Vertical thick gray lines show location of profiles, shown to scale and labeled at the top of each panel. D Profiles were not measured March 2003. Dashed line on A shows approximate location of central dividing wall prior to November 2001. Primary vent locations shown where identifiable. Small grid is 1-m squares, large grid is 5-m squares. Symbol key on figure. HC is hydrocarbon

in November 2001, large tar blocks (to 1.0×0.5×0.75 m) were observed in HC volcano #3 and the floor was sandy. By December 2001, the volcano floor of HC volcano #3 was comprised of pebbles and stones. In March 2003, seepage at HC volcano #0 was intense (but not dominant) and this small volcano's floor was pebbled.

Surveys after the transect chains were laid down showed one chain disappearing into walls of HC volcano #3, although elsewhere the chain remained atop the sediment. This strongly suggests that the HC volcano walls are

depositional features. Sediment in the volcano walls and floors is very cohesive due to the high tar content, yet the surveys showed walls were occasionally destroyed and also rebuilt. Thus, the northward “migration” of HC volcano #3 from March 2003 to June 2003 probably resulted from the destruction and rebuilding of its walls several meters to the north, and as a result, its walls were no longer penetrated by the transect chain in June 2003.

Not all volcano relocations were necessarily due to a destructive/constructive cycle, particularly with regards to HC volcano #4. By March 2003, HC volcano #4 was located on a plateau, with the seabed in the general area elevated several tens of centimeters. HC volcano #4 was first noted in March 2002 as a 2-cm-tall feature beyond HC volcano #3 and resembled a large, circular pancake rather than a volcano. A few sporadic bubble streams emerged from the feature. Over the next year it grew in height and gas emission. Seabed uplift to the west of HC volcano #3 and

**Table 1**

Summary of seabed morphology changes. See Fig. 5 for feature locations

Feature	#0	#1	#2	#3	#4	#5	E. Ridges	S. Ridge
Appearance	03/03	<11/00	<11/00	10/01	03/02	11/03	03/03	03/03
Movement	–	03/03	12/01	06/03	03/03	–	–	11/03
	04/03	3/03	–	06/03	–			
	11/03	11/03	–	11/03	–			
Growth	06/03	12/01	12/01	12/01	04/03	–	–	04/03
	06/03	03/02	03/02	–	–			
	–	06/03	–	–	–			
Shorter walls	–	10/01	10/01	04/03	06/03	–	–	06/03
	–	03/02	03/02	11/03				
	11/03							
Dominant volcano to seepage	06/03 to 11/03	11/00 to 10/01		11/01 to 04/03				

– implies no significant change, i.e., &lt;25%, or not applicable

of the plateau on which it stood accompanied this increase in seepage. However, in November 2003, HC volcano #4 was smaller than previous observations, and although still atop a plateau, the surrounding seabed was deeper than before. Simultaneously, HC volcano #4 and its plateau had shifted several meters to the south. These changes are more suggestive of the plastic deformation of tar saturated sediments than erosion and reformation.

Also suggestive of plastic deformation of the seabed are the ridge and ledge features. In general, tar ridges persisted for relatively short time periods. The south tar ridge (41 cm tall), first noted in March 2003, largely had disappeared by June 2003, replaced by a ledge in November 2003. Another example was the area to the north of HC volcano #3, which was noted as elevated only in the April 2003 survey. Seepage at tar ridges is much less than for the HC volcanoes, and they generally have slightly more seepage from their crests than their edges and the surrounding seabed.

Most elongated features were oriented north–south. During its initial growth phase, HC volcano #0 became highly oblong in a north–south direction, roughly centered on its primary vent. The east tar ridges and also the uplift between volcanoes #3 and #4 were north–south oriented. In one survey, HC Volcano #4 was north–south elongated, although in November 2003 it was roughly circular. HC volcano #0 had a unique, two-step profile on its southern wall in June 2003, with a raised plateau ~20 cm wide, halfway up (Fig. 5F). In November 2003, the profile for HC volcano #0 was still asymmetric, nearly vertical to the south and sloping towards the north.

Primary vent locations (marked with numbered rebar stakes) were generally persistent, although they were observed to move (or more likely deactivate with activation of a new primary vent), particularly when the HC volcano moves. Thus the main vents of HC volcanoes #1–#3 remained in the same location from November 2001 to March 2002; however, 1 year later (March 2003; Fig. 5D), they had shifted. At this time, the stakes marking vents #1 and #2 were found toppled over and were relocated by divers to the new vent locations.

Another change of note was the deposition of sand at the site prior to the April 2003 survey. The stake for vent #2 was found sticking ~15 cm out of the sandy seabed, instead of the ~50 cm during the previous survey, indicating the deposition of ~30 cm of sand (at least at vent #2). Ridges protruding above the sand matched the previous location of the walls of HC volcano #3, indicating other portions of HC volcano #3's walls were destroyed to a height less than the added sand overburden.

#### Turbine seep-tent

SCUBA divers deployed three turbine seep-tents (Fig. 1) at Shane Seep on March 11, 2003 (see Fig. 5D for locations). The tents were located in the peripheral zone in areas with three different seepage rates on an approximately level seabed. Thus, the tent skirts were flush with the seabed, sealing their interiors from the surrounding ocean. This zone was characterized by numerous small vents located ~30 to 50 cm apart, each producing lines of bubbles, and extended a few meters south and north of the transect chain. Vent density decreased further north, extending the furthest in the north-northeast directions, as far as 10 to 13 m. Deployment avoided the HC volcanoes on the hypothesis that fluxes might be large enough to lift the tents off the seabed.

Vertical temperature profiles were obtained during deployment and recovery (Fig. 6A). For each profile, data were depth segregated into 1-m depth layers and then averaged. The tents were deployed at 10:35 AM and the vertical profile showed a well-mixed water column, with a thin cooler layer near the seabed. Swell was low (~1 m) and predominantly from the south. Turbine data collection started at 11:00 AM and continued for 2 h once divers positioned the tents and attached the turbines. The seabed temperature and pressure are shown in Fig. 6B. By late morning, wind and swell had increased. These changes accompanied the arrival of a marine layer in the area, which arrived at the site at ~12:30 PM. At 13:10, the changing tide shifted the boat and pulled the turbines off the tents. Divers replaced the turbines at 13:50 and data collection resumed. Tent #3 was repositioned, slightly shifted from its original location, which may have caused

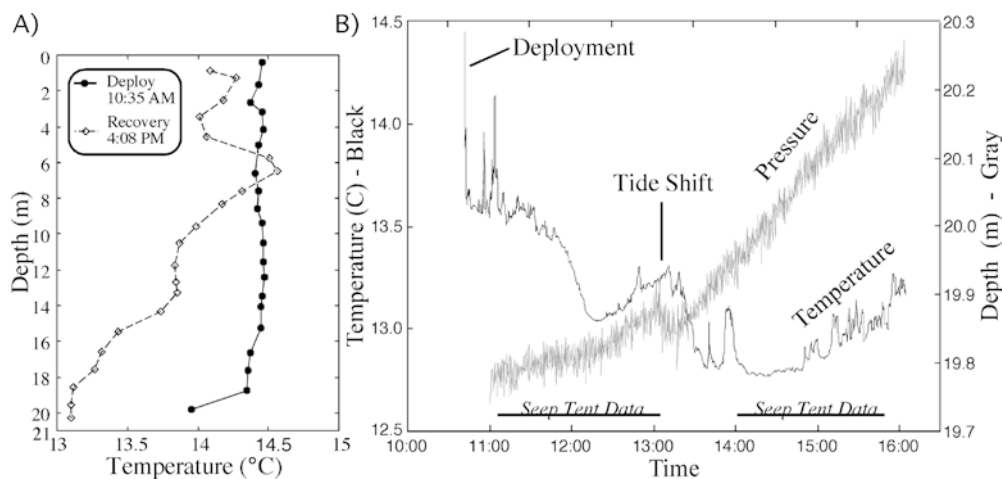


**Fig. 6** Vertical temperature profiles (1-m averaged) A and seabed temperature and pressure records B for March 11, 2003. Data key on figure, times of tide shift, deployment, and turbine data acquisition shown on B

an offset in its flux. The tide shift was accompanied by an influx of colder water at the seabed. Data collection continued for another 90 min before tent recovery due to the worsening weather. The vertical profile at recovery (Fig. 6A) showed cooler water throughout most of the water column.

Fluxes for the three tents are shown in Fig. 7. Variations on short time scales were observed; for example, there was a clear seepage response to hydrostatic pressure changes due to swell (Leifer and Boles 2004a). Interestingly, Tents #1 and #2 both experienced transient events termed “ejections,” during which the flux first decreased and then increased significantly. Raw data (not averaged or smoothed, i.e., 0.2-s resolution) for the ejection at tent #1 is shown in Fig. 8A. During this event,  $0.42 \text{ m}^3$  of gas (at STP) was emitted in  $\sim 5 \text{ s}$ . It is unclear if the high-frequency oscillations were real or a result of the turbulence within the turbine at such high flow rates. The calibration was extrapolated to this range because producing a gas flux of  $2 \text{ m}^3 \text{ min}^{-1}$  (at STP) was not achievable in the lab. Based on lab tests of smaller bubble pulses, the initial half second of rising flux most likely corresponds to the “bow wave”, or water pushed in front of the bubble, while some of the “tail” (14:13:55 to 14:13:57) likely resulted from persistence of the upwelling flow (or wake) after the

bubble pulse passed. Both immediately before the ejection and shortly afterwards, the gas flux dropped to zero for several seconds (Fig. 8A). The flux remained depressed for  $\sim 30 \text{ s}$  after the ejection before beginning to unsteadily recover to greater than its original value. A second ejection occurred at 12:08 PM at tent #2 (Fig. 8C) and showed a similar pattern, but with a smaller initiating drop, followed by recovery to a greater flux afterwards, at least for  $\sim 3 \text{ min}$ . The flux then decreased  $\sim 10\%$  and remained depressed for  $\sim 1 \text{ min}$ .

## Discussion

The turbine flux data shows variability with time scales from seconds to hours. On much longer time scales, seabed morphological changes occurred on monthly to yearly time scales. The high tar content of the sediment, and frequent construction/destruction of HC volcano features suggest that large ejections occur frequently and may often relate to tar. Leifer and Boles (2004b) concluded that small, very oily bubbles were formed occasionally during bubble formation and for high flow vents, during bubble breakup. Thus, we hypothesize that the dynamic nature of the COP

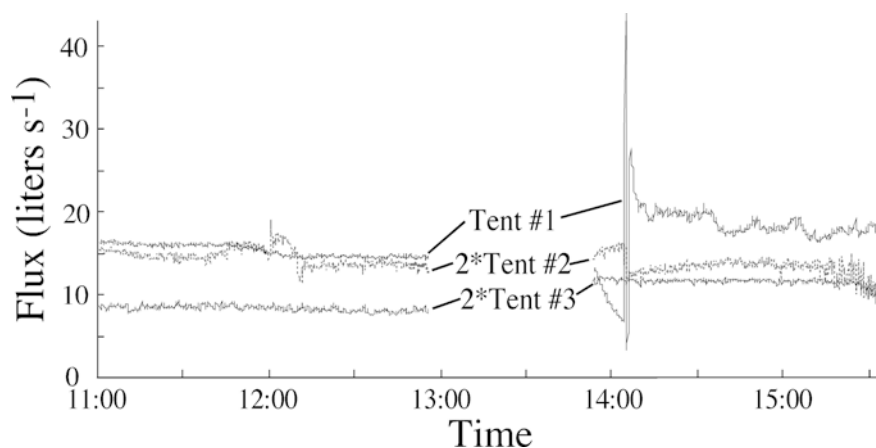


**Fig. 7** Flux, corrected to standard temperature and pressure ( STP). Tents labeled on figure

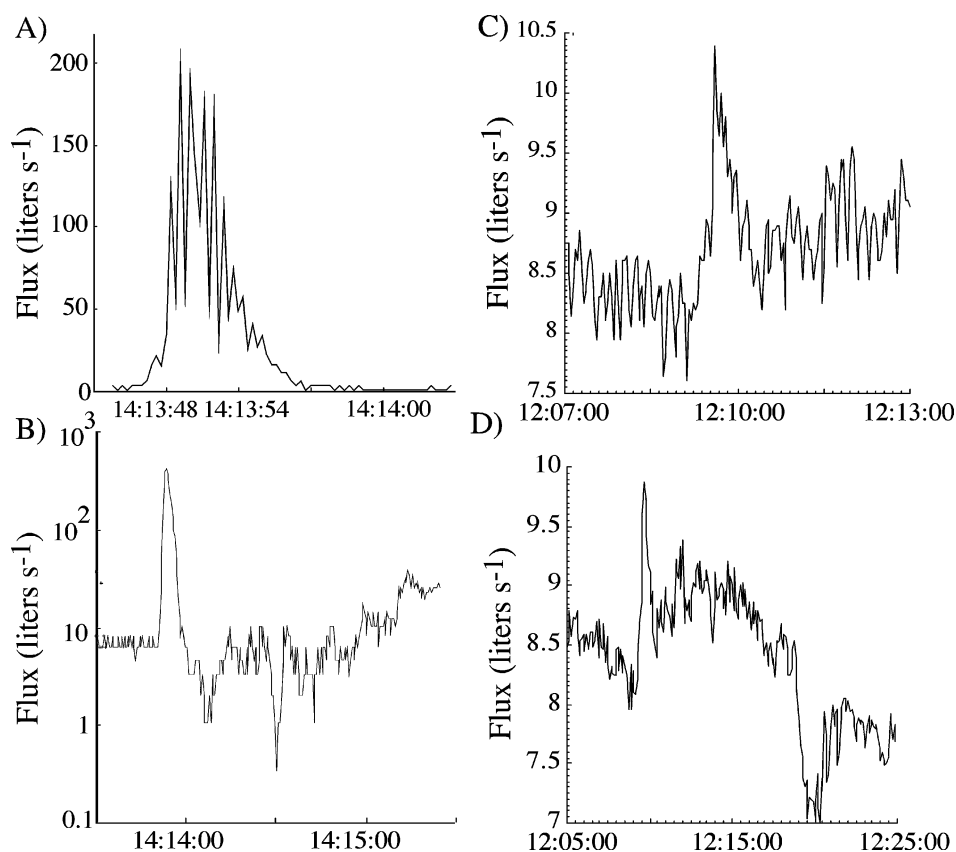


**Fig. 8**

Flux, corrected to standard temperature and pressure (STP), for A tent #1 during ejection event. Raw data with 0.2-s time resolution and B 1-s averaged data for tent #1. Note, vertical scale is logarithmic. C 1-s averaged data for tent #2 during a second ejection event and D 5-s averaged data for tent #2

Seep Field is due largely to the interplay between tar, oil, and gas.

#### Seep seabed-morphology

Seabed morphology changes over the years included the deposition of tar from ejections along with the removal of seabed material during large ejection events, plastic seabed deformation, and the erosion and burial of features by sand, probably during storms. Vent locations can remain fixed for years and then re-emerge nearby. While ejection events build up volcano walls, they also can destroy them. Together these changes provide strong evidence of the dynamic nature of hydrocarbon seeps.

#### Ephemeral nature of seabed seep features

HC volcano #3 formed during a 3-week period when ~10,000 kg of sediment was displaced (for 3.5-m diameter, 50-cm depth, and 2-g cm<sup>-3</sup> sediment density) and had highly circular walls that were centered on the main vent. This evolution is most plausibly explained by one or a series of “explosive” ejection events. During this period the walls of HC volcanoes #1 and #2 also were destroyed, indicating that ejections not only form HC volcanoes but also destroy them. Therefore, we propose that rapid formation of HC features including the growth of walls, or volcano relocation (i.e., destruction of the old walls and construction of new) provide evidence of frequent, powerful ejections or series of ejections. Further evidence of eruptive behavior is provided by the observation that when volcano walls grew taller, they grew symmetrically (except

for HC volcano #0) and buried the transect chain. Since we propose a depositional model for formation of these features, ejections are required to loft seabed material.

The magnitude of these events must have been significant. An ejection of orders of magnitude larger than shown in Fig. 8 was reported in Leifer and others (2003) and showed no significant modification of seabed features. Clearly, a very large event (or series of events) formed HC volcano #3. The blockage that caused the formation of HC volcano #3 could have been shallow or deep (deep is defined as many times the seep area size scale, i.e., >25 m). Any explanation must account for the destruction of the intervening ridge at the existing vents and the formation of HC volcano #3. One hypothesis is a shallow blockage of the flow through vents #1 and #2, which caused the pressure build-up necessary to form HC volcano #3. This pressure buildup and the subsequent formation ejected the large tar blocks found in HC volcano #3. Thus, the tar blocks suggest the most plausible mechanism was a tar plug. Since tar blocks were not found at the HC volcanoes #1 and #2, the tar probably was from the shallow subsurface under HC volcano #3.

Alternatively, we could hypothesize a deep source, such as a large gas pulse that upon reaching the seabed overwhelmed the capacity of the existing vents. This would lead to a pressure increase in the fractures underlying vents #1 and #2 which were too small to easily conduct the high gas flux. In this scenario, the pressure increased sufficiently to create a new pathway, i.e., HC volcano #3.

The blockage that caused the ejection event at tent #1 occurred sufficiently deep to stop seepage at all vents under the tent. Assuming the ejection at tent #2 was due to the same process (blockage and blow-through), then most likely the ejection only affected a fraction of the vents under the tent since the flux never ceased.

The ejection event at tent #1 released significant gas in a very short time, but did not significantly change seabed morphology. However, the event released tar (found on the bubble-breakup grid). This suggests that this type of ejection could contribute to the construction (via deposition and sand grain cementing) of HC volcano walls. The hypothesis that HC volcano walls form by a depositional process was dramatically demonstrated by the burial of the transect chain after it was draped across the newly formed HC volcano #3. Since elsewhere the chain, even two years later, lay on top of the sandy bottom, only a depositional process can explain the chain's disappearance into the volcano walls. Furthermore, the appearance of pebbles in the bottom of HC volcano #3's crater suggests that not only tar, but also sand and other fine unconsolidated sediment were lofted during these events, leaving behind the heavier pebbles.

#### Plastic seabed deformation

The seabed morphology surveys also showed changes that probably were not caused by eruptive events; namely seabed deformations including the appearance and relocation of tar ridges, ledges, and plateaus. These were most common towards the eastern edge of the seepage area, where there also was evidence of seabed uplift (~30 cm). We propose that these seabed deformations are related to tar (or very viscous oil) flows with minimal gas flux. In such case, the process is similar to tar oozes that form mounds at a beach tar seep at Carpinteria State Park, CA. This tar was used by indigenous peoples for boat making for centuries or longer (Fischer 1978). Given sufficient driving pressure, tar can migrate. At Shane Seep, this pressure probably results from gas trapped behind the tar, which may form gas spaces under the more transient seabed features. These features are associated with lower gas emissions, unlike the main HC volcanoes. The transience of these features may result from when gas becomes trapped underneath the tar-sand layer at the seep seabed or leaks faster than it is replaced from below. This may explain the subsidence west of HC volcano #4 in November 2003 as compared to previous surveys, which occurred during a period when its size decreased significantly. Because tar is deformable, pressure relief could be lateral, thereby causing seabed surface features to shift, as happened between April and June 2003.

A major difference in the formation of HC volcanoes #3 and #4 was that HC volcano #4 formed gradually (over a year) and included a raised plateau, while HC volcano #3 appeared suddenly. Not only did the plateau height gradually increase with time, but the gas flux at HC volcano #4 and the size and height of its walls also increased gradually. When first identified, HC volcano #4 was only a few centimeters tall and emitted a few bubble streams. By 2003, its crater was meters across with walls half a meter high

and many active vents. This is consistent with the tar initially being slowly forced from the fractures until the gas flux was sufficiently great (i.e., fractures were sufficiently open) to begin ejecting tar and forming walls. Also interesting and probably tar related was the "death" of HC volcano #3, which was preceded by relocation of the volcano to north of the transect chain. This probably signifies that tar had begun blocking the fractures under HC volcano #3 and was no longer being effectively cleared through by the gas flux. Gas flux then shifted to other vents (#0 and #4 in April 2003), while HC volcano #3 migrated north a few meters. This shift could have been as a result of this tar blockage not being cleared. Alternatively, the shift in gas flux could have stopped further clearing of tar plugs by the blow-through ejection mechanism. Furthermore, an increase in tar flux and blockage of pathways could explain the large (~50 cm) increase in plateau height near HC volcano #3 during the same period, prior to the expansion of HC volcano #4 between April and June 2003.

#### Seep ejections and bubble survivability

##### Net effect of ejections on total flux

The 5-s ejection at tent #1 released 140 l of gas (at 3 bar), in comparison to the prior background flux of  $5.3 \text{ l s}^{-1}$ . Thus the ejection released gas equivalent to 26 s of normal flux in just 5 s. Since total flux dropped to  $\sim 3 \text{ l s}^{-1}$  (at 3 bar) for several minutes before the ejection, the total effect of the ejection was a net decrease in flux. However, afterwards the flux increased and remained elevated (~25%) for tens of minutes. Including the post ejection increase in flux yields a clear net increase in gas flux. The key point is that the ejection flux itself did not significantly impact overall flux at tent #1. Rather it was the changes before and afterwards that had a significant effect (which we hypothesize were due to tar) for the vents under tent #1. What remains unknown is whether the overall flux for the entire seep domain was significantly altered, or simply shifted between vents. These observations suggest that the larger events associated with changes in seabed morphology may also significantly enhance seep gas emissions. However, since this conclusion is based on extrapolation, further research is required to determine if the eruptive gas ejection for these larger events which significantly change seabed features, contribute significantly to total gas flux.

##### Ejections and bubble survival

Bubble plumes from low flow vents in the Gulf of Mexico (Leifer and MacDonald 2003) and Santa Barbara Channel (Leifer and Boles 2004b) produced a narrow size range, while bubble plumes from high flow vents produced a wide spectrum of bubble sizes including very large and very small bubbles. Not surprisingly, high flow vents also generated stronger upwelling flows. Higher flux seeps in the COP seep field enhance the dissolved methane concentrations in the plume water surrounding the bubbles, thereby decreasing the bubble dissolution rate (Clark and others 2003). In numerical studies, Leifer and Patro (2002) showed that upwelling flows and enhanced plume methane

concentrations increase bubble survivability and vertical, bubble-mediated methane transport. Bubble emission size distributions during ejection events are unknown, but since they are high flow, they most likely produce a broad, weakly size dependent, bubble size-distribution, extending to very large bubbles. The lab test pulses produced bubbles as large as tens of centimeters. The higher flux and broader size range should significantly enhance methane concentrations in the plume water. Upwelling flows would also be stronger given the greater bubble flux. These three factors lead to the hypothesis that bubble-mediated gas transport to the sea surface from large transient ejection events will be much greater than for an equivalent flux from more widespread and non-ejective gas emissions.

### A proposed mechanism for transient behavior of seeps

An electrical network model

Seep vents are probably interconnected in a complex manner through subsurface fractures, faults, unconsolidated sediment, and rocks. A simplified approach to model subsurface gas seepage is as a network of connected resistors with resistances  $R_j$  - equivalent to viscosity, and capacitors with capacitances  $C_j$  - equivalent to reservoirs or fracture capacities, driven by a voltage potential,  $V_R$  - equivalent to the system overpressure (Fig. 9A). If  $V_R$  changes (e.g., due to an increase in water column height or reservoir pressure), the flow for each pathway—equivalent to current  $i_j$ , adjusts with its own time scale until a new equilibrium flow is achieved. The new equilibrium will have a different ratio of flow for each vent from the original equilibrium due to the relationship between viscosity and flow. This is analogous to the change in resistance in a resistor due to heating from changes in current. Continuing the analogy, larger pathways (equivalent to higher wattage resistors) are more capable of conducting an increased flow with less of an increase in viscous damping (corresponding to less resistive heating) than smaller pathways. This is consistent with the observations

of Leifer and Boles (2004b) that the vent with the highest flow showed the smallest response to swell-induced flow variations. The response of the fracture system is complex, with each fracture acting as a low pass filter with its own  $RC$  time constant. Thus, high capacity and high resistance fractures (long  $RC$  time constant) damp out variations, while low capacity and low resistance fractures (short  $RC$  time constant) do not. However, an amplified response to the driving pressure signal, as reported for swell pressure forcing in Leifer and Boles (2004b) requires a more complex model. Leifer and Boles (2004b) proposed pore activation and deactivation as the most likely process. In their model, pores are activated and deactivated depending upon the vent overpressure required to overcome surface tension and hydrostatic pressure to form bubbles. In our electrical analog model, this is equivalent to a Zener diode at each vent mouth that blocks current flow unless a certain voltage potential is exceeded.

The model shown in Fig. 9A is for gas only. In reality, there should be a second electrical network to describe the oil flux, which shares the same pathways. Moreover, interconnections between the two networks likely are numerous and intimate. As an example, consider an increase in gas flow. This increases the driving force behind the oil flow, increasing the oil flow. This is analogous to a transistor in which a current applied to the gate (gas flow) controls the current flow between the base and emitter (oil flow), shown in Fig. 9B. Alternatively, if the initiating event is an increase in oil flow, the fracture dimensions will be reduced and thus the resistance to gas flow increases and fracture capacity decreases. This leads to higher driving pressure ( $V_R$ ) that further increases the oil flow, depleting the oil reservoir in that portion of the fracture. Oil depletion then leads to a reduced oil flow. Thus, many of these feedback cycles lead to oscillatory behavior. Leifer and Boles (2004b) reported a 4-Hz frequency oscillation in bubble gas emissions from a single low flow vent at Shane Seep. They proposed this resulted from the interaction between the oil and gas flows.

One prediction of the resistance model is that not only do decreases or increases in resistance in one fracture cause a

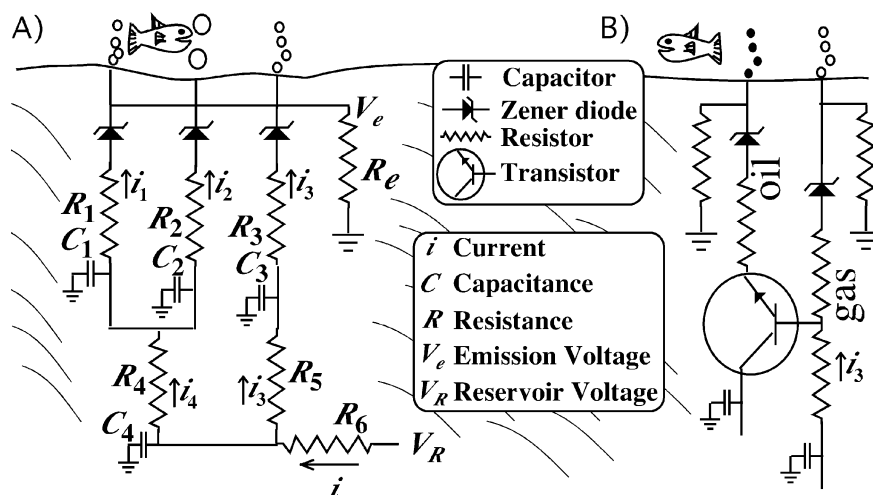


Fig. 9

Electrical network analogue for subsurface hydrocarbon seepage. A shows gas seepage, B shows oil-gas interaction. Symbol key on figure

change in the distribution of flow (current) through the various fractures (resistors) in the seep domain; but the total flow also changes. Another prediction, is that there is an asymmetry in the readjustment between flow increases and decreases in the fractures due to the non-linear effect of viscosity (resistive heating). Increases shift equilibrium towards higher flow vents (less viscous damping—higher wattage resistor) while decreases shift equilibrium towards lower flow vents (lower wattage resistor) since there is less viscous damping at lower flow rates. The asymmetry arises since large fractures have less resistance to bubble formation (i.e., smaller Zener diodes).

#### A tar migration and formation model

The proposed electrical network model allows investigation of the response, including equilibrium shifts, of the fracture system to external and internal driving forces and processes; however, it cannot explain large transient events (e.g., Fig. 8A). During the 5-h data set, two ejection events were observed. The numerous significant seabed morphology changes also suggest that much larger, but unobserved, transient events occur. The symmetric shape of the HC volcano walls and the burial of the transect chain by wall-growth support an eruptive formation process in which tar cements sand grains together, forming the volcano walls. We propose that tar has the capability to change fracture dimensions, and unlike oil, does not readily flow—i.e., tar migration is likely “punctuated,” particularly if it blocks fractures until increasing pressure blows clear the tar plug.

In our model, gas bubbles flow through the center of narrow portions of the fracture system—bottle-necks—where the oil is driven primarily along the fracture walls. Because the velocity must decrease to zero at the walls—by continuity, oil adjacent to the walls (in a boundary layer) is nearly stationary. As a result, oil ages (from biodegradation or loss of volatiles into the gas flow) in the fractures, becoming more viscous and less mobile. Biodegradation has been inferred at the reservoir level beneath Platform Holly (Orphan and others 2003) and deep subsurface in the Gulf of Mexico (Sassen and others 2003). As oil ages it becomes less and less mobile until it becomes immobile tar on the fracture wall. This process gradually narrows the fracture, particularly in the bottle-necks, increasing the resistance and thus the pressure ( $V_R$ ) across the developing blockage. In the electrical model, this causes a decrease in the gas and oil flows. Eventually, the fracture blockage is sufficient that the pressure across the blockage blows the tar clear, or creates a new pathway, bypassing the original fracture and blockage point. During this violent decompression, tar in other portions of the fracture network also may be blown free. The blow-through depressurizes the portion of the fracture behind the blockage point, thus the flow decreases precipitously. Once the flow recovers, it does so at a higher magnitude due to the lower resistance of the now clearer, and hence more open, fracture. The tar blown free may reach the seabed and escape to the ocean (as on the bubble breakup grid of tent #1) or lodge elsewhere in the fracture network, thereby either partially, or completely blocking the

fracture at another bottleneck and leading to a repetition of the blockage and blow-through process. Thus, in this model, tar migrates in discrete events and is blown upwards from one fracture constriction to another.

## Conclusions

This paper shows the highly dynamic behavior of a shallow marine hydrocarbon seep, including both spatial and temporal variability on a wide range of scales. Understanding the mechanisms underlying these observations requires time and spatial flux measurements. To understand this variability, new approaches were developed, including a network of turbine seep-tents that allows long-term spatial and temporal observations of discharge rates, and mapping of the spatial and temporal variability in seabed features and vent locations. However, given the probable violence of the largest transient events, it is unlikely that as designed, the tents would survive. Still, insight into these processes can be gained from the tent observations.

We present an electrical model analog of subsurface hydrocarbon seepage that is useful for interpretation of both the spatial and temporal variability of seepage in terms of “the subsurface plumbing system.” We also propose a model of the interaction of tar with oil and gas seepage.

Seepage varies by many orders of magnitude on time scales from sub-second to decadal with variability including large transient seepage events. Transient events produce greater bubble fluxes with likely broader bubble size-distributions, increased upwelling flows, and elevated aqueous-plume methane concentrations. For these reasons, we propose that large transient gas emissions enhance, potentially significantly, marine-seep methane flux to the atmosphere.

For Shane Seep, tar blockage of seep conduits was proposed to play an important role in modulating transient events. Thus where seepage is associated with petroleum deposits, such as the Gulf of Mexico and other oil producing basins, similar transient behavior is likely. Similar behavior may occur under other conditions, for example, clay could play a similar role to tar, causing modulation of seepage and transient emissions.

Understanding the transient behavior of hydrocarbon seepage is critical for assessing synoptic measurements of hydrocarbon seepage. Specifically, how representative are quantitative estimates made at a single time with respect to the temporal average? While long-term monitoring of individual seep vents is an important step in understanding the temporal variability of seepage, variability in seabed morphology suggests that long-term trends cannot be interpreted without a broader, spatial context. Finally, for prediction of the impact of transient events on the global atmospheric methane budget, measurements of the ambient conditions during ejections, including upwelling flow, plume saturation, and bubble distributions are critical.

**Acknowledgments** We would like to thank the support of the U.S. Mineral Management Service, Agency #1435-01-00-CA-31063, Task #18211 and the University of California Energy Institute. Special thanks to University of California, Santa Barbara (UCSB) divers Shane Anderson, Dave Farrar, Dennis Divins, and underwater videographer Eric Hessel. The views and conclusions in this document are those of the authors and should not be interpreted as necessarily representing the official policies, either expressed or implied of the U.S. government or UCSB.

## References

- Allen AA, Schlueter RS, Mikolaj PG (1970) Natural oil seepage at Coal Oil Point, Santa Barbara, California. *Science* 170:974–977
- Blanchard DC, Syzdek LD (1977) Production of air bubbles of a specified size. *Chem Eng Sci* 32:1109–1112
- Boles JR, Clark JF, Leifer I, Washburn L (2001) Temporal variation in natural methane seep rate due to tides, Coal Oil Point area, California. *J Geophys Res* 106C11:27077–27086
- Cicerone RJ, Oremland RS (1988) Biogeochemical aspects of atmospheric methane. *Global Biogeochem Cycles* 2:299–327
- Clark JF, Leifer I, Washburn L, Luyendyk BP (2003) Compositional changes in natural gas bubble plumes: observations from the Coal Oil Point Seep Field. *Geo-Mar Lett* 23:187–193
- Clark JF, Washburn L, Hornafius JS, Luyendyk BP (2000) Dissolved hydrocarbon flux from natural marine seeps to the southern California Bight. *J Geophys Res* 105:11509–11522
- Clester SM, Hornafius JS, Scepan J, Estes JE (1996) Quantification of the relationship between natural gas seepage rates and surface oil volume in the Santa Barbara Channel. *EOS Trans Am Geophys Union* 77:420
- Clift R, Grace JR, Weber ME (1978) Bubbles, drops, and particles. Academic Press, New York, 380 pp
- Crutzen PJ (1995) The role of methane in atmospheric chemistry and climate. In: Engelhardt WV, Leonhardt-Marek S, Breves G, Giesecke D (eds) Ruminant physiology: digestion, metabolism, growth and reproduction. Proceedings of the Eighth International Symposium on Ruminant Physiology. Ferdinand Enke Verlag, Stuttgart, pp 291–315
- De Beukelaer SM, Guinasso NL Jr, MacDonald IR, Murray JA (2003) Distinct side-scan sonar, RADARSAT SAR, and acoustic profiler signatures of gas and oil seeps on the Gulf of Mexico slope. vol 23, pp 177–186
- Etiopie G, Klusman RW (2002) Geologic emissions of methane into the atmosphere. *Chemosphere* 49:779–791
- Fischer PJ (1978) Natural gas and oil seeps, Santa Barbara Basin, California. California offshore gas, oil, and tar seeps. State Lands Commission, prepared by the Staff of the State Lands Commission, Sacramento, CA, pp 1–62
- Fischer PJ, Stevenson AJ (1973) Natural hydrocarbon seeps, Santa Barbara basin, California, Santa Barbara Channel area revisited. Fischer PJ (ed) Field trip guidebook, vol 3. Am Assoc Petrol Geol, Tulsa, Oklahoma, pp 17–28
- Gal-Or B, Waslo S (1968) Hydrodynamics of an ensemble of drops (or bubbles) in the presence or absence of surfactants. *Chem Eng Sci* 23:1431–1446
- Hornafius JS, Quigley D, Luyendyk BP (1999) The world's most spectacular marine hydrocarbon seeps (Coal Oil Point, Santa Barbara Channel, California): quantification of emissions. *J Geophys Res* 104:20703–20711
- Hovland M, Judd AJ, Burke RA (1993) The global flux of methane from shallow submarine sediments. *Chemospheres* 26:559–578
- Judd AG, Hovland M (1992) The evidence of shallow gas in marine sediments. *Cont Shelf Res* 12:1081–1095
- Judd AG, Hovland M, Dimitrov LI, Garcia GS, Jukes V (2002) The geological methane budget at Continental Margins and its influence on climate change. *Geofluids* 2:109–126
- Katz ME, Pak DK, Dickens GR, Miller KG (1999) The source and fate of massive carbon input during the latest Paleocene thermal maximum. *Science* 286:1531–1533
- Kennett JP, Cannariato KG, Hendy IL, Behl RJ (2000) Carbon isotopic evidence for methane hydrate instability during quaternary interstadials. *Science* 288:128–133
- Kennett JP, Cannariato KG, Hendy IL, Behl RJ (2003) Methane hydrates in Quaternary climate change: the clathrate gun hypothesis. AGU Washington, vol. 54, 216 pp
- Kvenvolden KA, Reeburgh WS, Lorenson TD (2001) Naturally occurring methane seepage—workshop report. *EOS* 82:457
- La Montagne MG, Leifer I, Bergmann S, Vandewerhorst LC, Holden PA (2004) Bacterial diversity in marine hydrocarbon seep sediment. *Environ Microbiol* (in press)
- Leifer I, Boles J (2004a) Turbine seep-tent measurements of marine hydrocarbon seep forcing on sub-hourly time scales. *J Geophys Res* (in press)
- Leifer I, Boles J (2004b) Measurement of hydrocarbon flow through fractured rock and unconsolidated sediment of a marine seep. *Marine Petroleum Geology* (in press)
- Leifer I, Clark J, Chen R (2000b) Modifications of the local environment by a natural marine hydrocarbon seep. *Geophys Res Lett* 27:3711–3714
- Leifer I, Clark JF (2002) Modeling trace gases in hydrocarbon seep bubbles: application to marine hydrocarbon seeps in the Santa Barbara Channel. *Russ Geol Geophys* (English translation published by the American Geophysical Union) 47:572–579
- Leifer I, Clark JF, Luyendyk B, Valentine D (2003) Identifying future directions for subsurface hydrocarbon migration research. *EOS* 84:364–371
- Leifer I, Judd AG (2002) Oceanic methane layers: a bubble deposition mechanism from marine hydrocarbon seepage. *Terra Nova* 16:471–425
- Leifer I, Luyendyk BP, Broderick K (2004) Tracking an oil slick through an area with multiple natural sources, Coal Oil Point, California. AAPG Memoir (submitted)
- Leifer I, MacDonald I (2003) Dynamics of the gas flux from shallow gas hydrate deposits: interaction between oily hydrate bubbles and the oceanic environment. *Earth Planet Sci Lett* 210:411–424
- Leifer I, Patro R (2002) The bubble mechanism for transport of methane from the shallow seabed to the surface: a review and sensitivity study. *Cont Shelf Res* 22:2409–2428
- Leifer I, Patro R, Bowyer P (2000a) A study on the temperature variation of rise velocity for large clean bubbles. *J Atmos Ocean Tech* 17:1392–1402
- MacDonald IR, Boland GS, Baker JS, Brooks JM, Kennicutt II MC, Bidigare RR (1989) Gulf of Mexico chemosynthetic communities II: spatial distribution of seep organisms and hydrocarbons at Bush Hill. *Mar Biol* 101:235–247
- MacDonald IR, Buthman DB, Sager WW, Peccini MB, Guinasso JR NL (2000) Pulsed flow of oil from a mud volcano. *Geology* 28:10907–10910
- MacDonald IR, Leifer I, Sassen R, Stine P, Mitchell R, Guinasso JR N (2002) Transfer of hydrocarbons from natural seeps to the water column and atmosphere. *Geofluids* 2:95–107
- Mader HM, Brodsky EE, Howard D, Sturtevant B (1997) Laboratory simulations of sustained volcanic eruptions. *Nature* 388:462–464
- McDougal TJ (1978) Bubble plumes in stratified environments. *J Fluid Mech* 4:655–672
- Mikolaj PG, Ampaya, JP (1973) Tidal effects on the activity of natural submarine oil seeps. *Mar Tech Soc J* 7:25–28
- Milkov AV (2000) Worldwide distribution of submarine mud volcanoes and associated gas hydrates. *Mar Geol* 167:29–42

- Milkov AV, Sassen R, Apanasovich TV, Dadashev FG (2003) Global gas flux from mud volcanoes: a significant source of fossil methane in the atmosphere and the ocean. *Geophys Res Lett* 30:1037–1038
- Orphan VJ, Goffredi SK, Delong EF, Boles JR (2003) Geochemical influence on diversity and microbial processes in high-temperature reservoirs. *Geomicrobiol J* 20:295–311
- Patro RK, Leifer I, Bowyer P (2001) Better bubble process modeling: improved bubble hydrodynamics parameterisation. In: Donelan M, Drennan W, Salzman ES, Wanninkhof R (eds) Gas transfer and water surfaces, vol. 127. AGU Monogr, pp 315–320
- Prather M, Derwent R, Ehhalt D, Fraser P, Sanhueza E, Zhou X (1995) Other trace gases and atmospheric chemistry. In: Houghton JT, Meira Filho LG, Bruce J, Lee H, Callander BA, Haites E, Harris N, Maskell (eds) Climate change 1994: radiative forcing of climate change and an evaluation of the IPCC IS92 emission scenarios. Cambridge University Press, Cambridge, pp 73–126
- Quay P, Stutsman J, Wilbur D, Snover A, Dlugokencky E, Brown T (1999) The isotopic composition of atmospheric methane. *Global Biogeochem Cycles* 13:445–461
- Quigley DC, Hornafius JS, Luyendyk BP, Francis RD, Clark J, Washburn L (1999) Decrease in natural marine hydrocarbon seepage near Coal Oil Point, California, associated with offshore oil production. *Geology* 27:1047–1050
- Rehder G, Brewer PW, Peltzer ET, Friederich G (2002) Enhanced lifetime of methane bubble streams within the deep ocean. *Geophys Res Lett* 29:1731–1746
- Rehder G, Keir RS, Suess E, Rhein M (1999) Methane in the northern Atlantic controlled by microbial oxidation and atmospheric history. *Geophys Res Lett* 26:587–590
- Rowland FS (1985) Methane and chlorocarbons in the earth's atmosphere. *Origins of Life* 15:279–297
- Sassen R, Milkov A, Ozgul E, Roberts HH, Hunt JL, Beeunas MA, Chanton JP, DeFreitas DA, Sweet S (2003) Gas venting and subsurface charge in the Green Canyon area, Gulf of Mexico continental slope: evidence of a deep bacterial methane source? *Organic Geochem* 34:1455–1464
- Slauenwhite DE, Johnson BD (1999) Bubble shattering: differences in bubble formation in fresh water and seawater. *J Geophys Res* 104:3265–3276
- Sokolov VA, Buniat-Zade ZA, Geodekian AA, Dadashev FD (1969) The origin of gases and mud volcanoes and the regularities of their powerful eruptions. In: Schenk PA, Havenaar I (eds) Advances in geochemistry. Pergamon, Oxford, pp 473–484
- Tryon MD, Brown KM, Torres ME, Trehu AM, McManus J, Collier RW (1999) Measurements of transience and downward fluid flow near episodic methane gas vents, Hydrate Ridge, Cascadia Geol 27:1075–1078
- Tsunogai U, Yoshida N, Ishibashi J, Gamo T (2000) Carbon isotopic distribution of methane in deep-sea hydrothermal plume, Myojin Knoll Caldera, Izu-Bonin arc: implications for microbial methane oxidation in the oceans and applications to heat flux estimation. *Geochim Cosmochim Acta* 64:2439–2452
- Valentine DL, Blanton DC, Reeburgh WS, Kastner M (2001) Water column methane oxidation adjacent to an area of active hydrate dissociation. Eel River Basin. *Geochim Cosmochim Acta* 65:2633–2640
- Wanninkhof R (1992) Relationship between wind speed and gas exchange over the ocean. *J Geophys Res* 97C5:7373–7382
- Washburn L, Clark JF, Kyriakidis P (2004) The spatial scales, distribution, and intensity of natural marine hydrocarbon seeps near Coal Oil Point, California. *Marine Petroleum Geology* (in press)
- Washburn L, Johnson L, Gotschalk CG, Eglund ET (2001) A gas-capture buoy for measuring bubbling gas flux in oceans and lakes. *J Atmos Oceanic Tech* 18:1411–1420
- Watanabe S, Tsurushima N, Kusakabe M, Tsunogai S (1995) Methane in Izena Cauldron, Okinawa Trough. *J Oceanogr* 51:239–255
- Woolf DK, Thorpe SA (1991) Bubbles and the air-sea exchange of gases in near saturation conditions. *J Mar Res* 49:435–466